Electronic Supplementary Material (ESI) for Journal of Materials Chemistry A.

The Nature of Methylamine-$MAPbI_3$ Complex: Fundamentals of Gas-Induced Perovskite Liquefaction and Crystallization

Dmitry Bogachuk[1,2], Lukas Wagner[1,2], Simone Mastroianni[1,3], Michael Daub[4], Harald Hillebrecht[3,4] and Andreas Hinsch[1*]

[1] Fraunhofer Institute for Solar Energy Systems ISE, Freiburg, 79110, Germany
[2] Laboratory for Photovoltaic Energy Conversion, Albert-Ludwigs-Universität Freiburg, Freiburg, 79110, Germany
[3] Materials Research Center FMF, Albert-Ludwigs-Universität Freiburg, 79104 Freiburg, Germany
[4] Institute for Inorganic and Analytic Chemistry, Albert-Ludwigs-Universität Freiburg, 79104 Freiburg, Germany

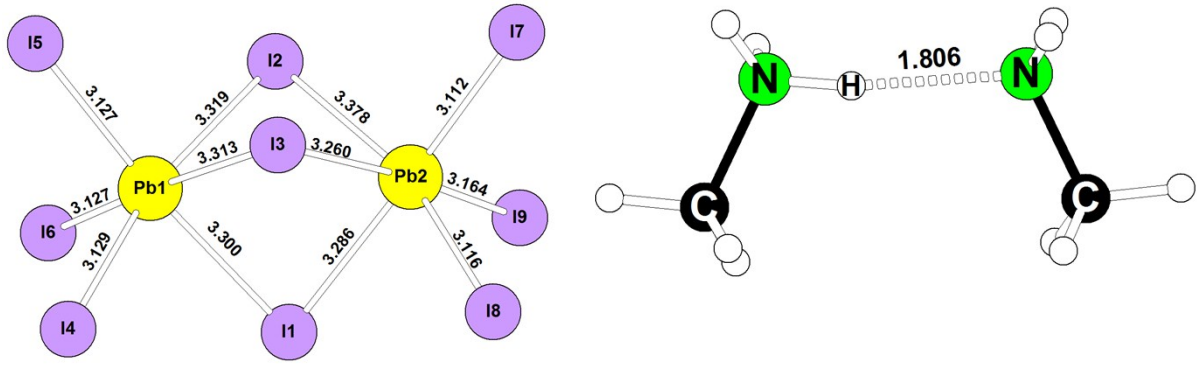

Figure S1: Visualized representation of building units $[Pb_2I_9]^{5-}$ and $[CH_3NH_3CH_3NH_2]^{+}$ in $(CH_3NH_3)_5(CH_3NH_2)_2Pb_2I_9$ based on the obtained XRD data

Table S1: Crystallographic data of $(CH_3NH_3)_5(CH_3NH_2)_2Pb_2I_9$, $Pb(CH_3NH_2)_4I_2$ and $Pb(CH_3NH_2)_6I_2$ estimated standard deviations in parentheses

Compound	$(CH_3NH_3)_5(CH_3NH_2)_2Pb_2I_9$	$Pb(CH_3NH_2)_4I_2$	$Pb(CH_3NH_2)_6I_2$
Temperature	100 K		
Crystal system	monoclinic	monoclinic	cubic*
Space group	$P\,2_1/c$	$P\,2_1/c$	$Fm3m$
Unit cell in [Å]	a = 13.7676(14)	a = 8.5684(2)	a = 10.487(7)
	b = 14.8730(14)	b = 12.6121(3)	
	c = 19.0855(19)	c = 13.3607(3)	
	β = 110.585(4)°	β = 98.877(1)°	
	Z = 4	Z = 4	Z = 4
$d_{calc.}$	3.233 g/cm³	2.725 g/cm³	2.208 g/cm³
Radiation	Mo-Kα;, microsource		
Data collection	Bruker, APEX II, CCD		
2Θ max	60°	87.4°	60°
	$-19 < h < 0$	$-16 < h < 16$	$-17 < h < 17$
	$-15 < k < 11$	$-24 < k < 24$	$-17 < k < 17$
	$-14 < l < 22$	$-25 < l < 25$	$-17 < l < 17$
μ	16.80 mm^{-1}	16.12 mm^{-1}	11.83 mm^{-1}
Absorption correction	multiscan, program SADABS[1]		
$R_{int.}$ / R_{sigma}	0.024 / 0.044	0. 062/ 0.039	0.085 / 0.021
Refinement	SHELXTL[2]		
N(hkl) meas.; unique	6651, 4470	89003; 10940	7344; 187
N'(hkl) (I > 2σ(I))	3751	8601	179
Parameters refined	171	104	8
R-values	$R_1(F)$ = 0.052, w$R_2(F^2)$= 0.138	$R_1(F)$ = 0.029, w$R_2(F^2)$= 0.050	R_1 = 0.065, w$R_2(F^2)$ = 0.175
all data	R_1 = 0.062	R_1 = 0.048	R_1 = 0.067
Weighting scheme[2]	0.0104 / 3.58	0.0127 / 2.2762	0.08/ 200
Extinction correction[2]	0.00024(4)	–	0.0014(5)
Goodness of fit	0.939	1.026	1.287
Residual electron density (max., min., sigma)	3.77/ – 2.72/ 0.29 e$^-$/Å^3	1.87/ – 2.65/ 0.26 e$^-$/Å^3	2.82 / – 2.31/ 0.39 e$^-$/Å^3

* at 100 K the crystal shows multiple twinning with a close relation to a cubic parent structure. As a result the profiles were split. For each reflection up to eight maxima were observed with more or less overlapping. It was impossible to assign individual orientation matrices in order to describe the diffraction pattern as a sum of separated twin domains. Because no super structure reflections were observed, the data set was integrated assuming an F-centred unit cell with $a \approx 10.5$ Å and merged in Laue class m3m.

[1] G. M. Sheldrick, Program SAINT, Bruker Analytical X-ray Systems, Madison, Wisconsin, USA, **2006**.; Program SADABS, University of Göttingen, Germany, **1996.**

[2] G. M. Sheldrick, *SHELXTL, Crystallographic System*, Bruker AXS Analytical X–ray Instruments Inc., Madison, **2013.**

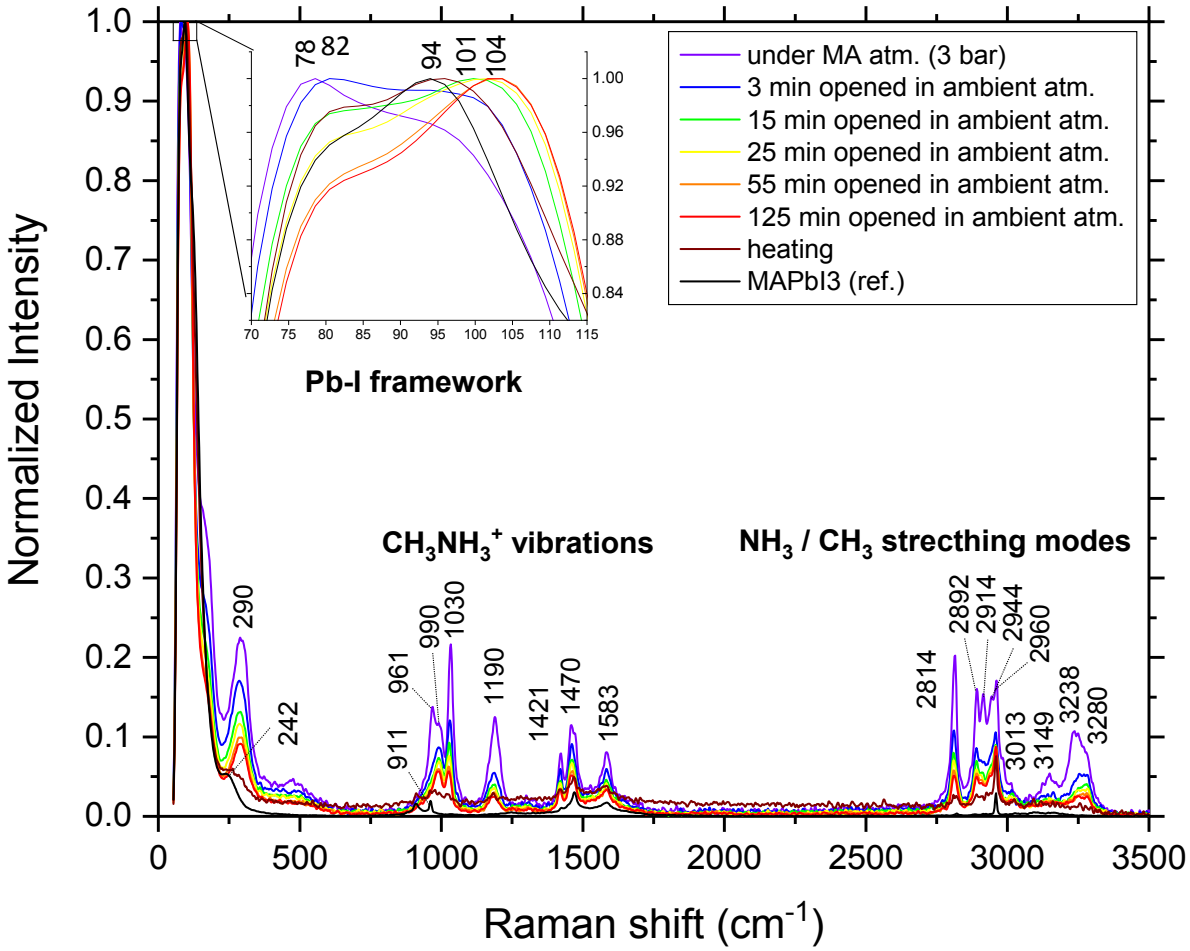

Figure S2: Complete Raman spectrum, with identification of band regions. The inset shows the gradual band shift during the crystallization in the low-wavenumber region.

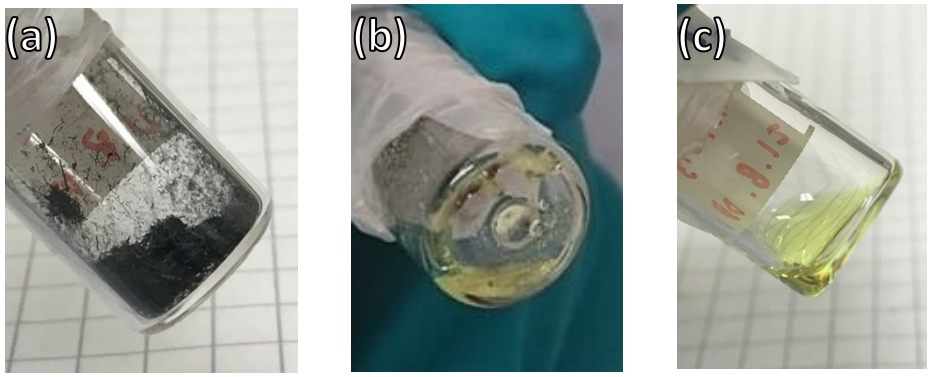

Figure S3: The process of $MA^0xMAPbI_3$ complex formation in a closed vial. (a) initial $MAPbI_3$ powder (b) viscous $MA^0xMAPbI_3$ (c) $MA^0xMAPbI_3$ diluted in ACN

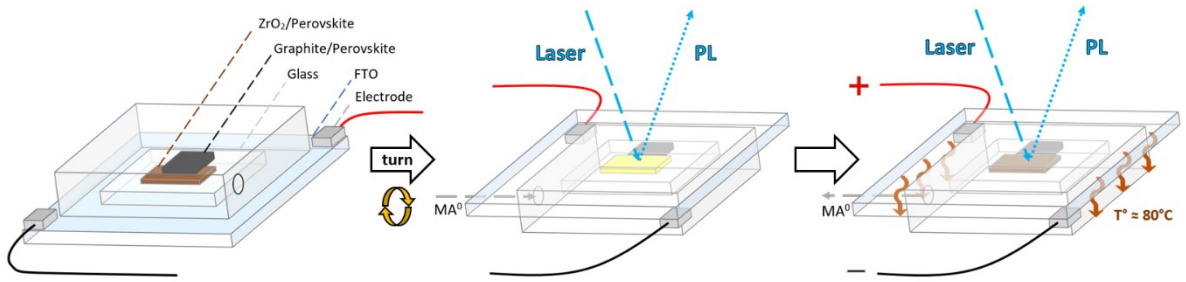

Figure S4: Schematic representation of the setup during the real-time PL measurement of the liquefaction and recrystallization

A transparent FTO-plate connected to a power supply was placed on the bottom side of the transparent chamber with ZrO_2 and Graphite layers filled with perovskite in it. The real-time PL measurement starts once the chamber is turned, and the PL originating from the radiative charge carrier recombination is detected by camera. Immediately, methylamine gas is supplied, causing a liquefaction of $MAPbI_3$ and loss of photoluminescence. After a small outlet is opened, methylamine gas starts to leave the liquefied complex reforming the perovskite structure. Furthermore, the supplied electrical current flowing through the FTO-plate is dissipated through heat, thus acting as a transparent annealing hotplate for the perovskite in the ZrO_2/Graphite layers with T = 70°C.

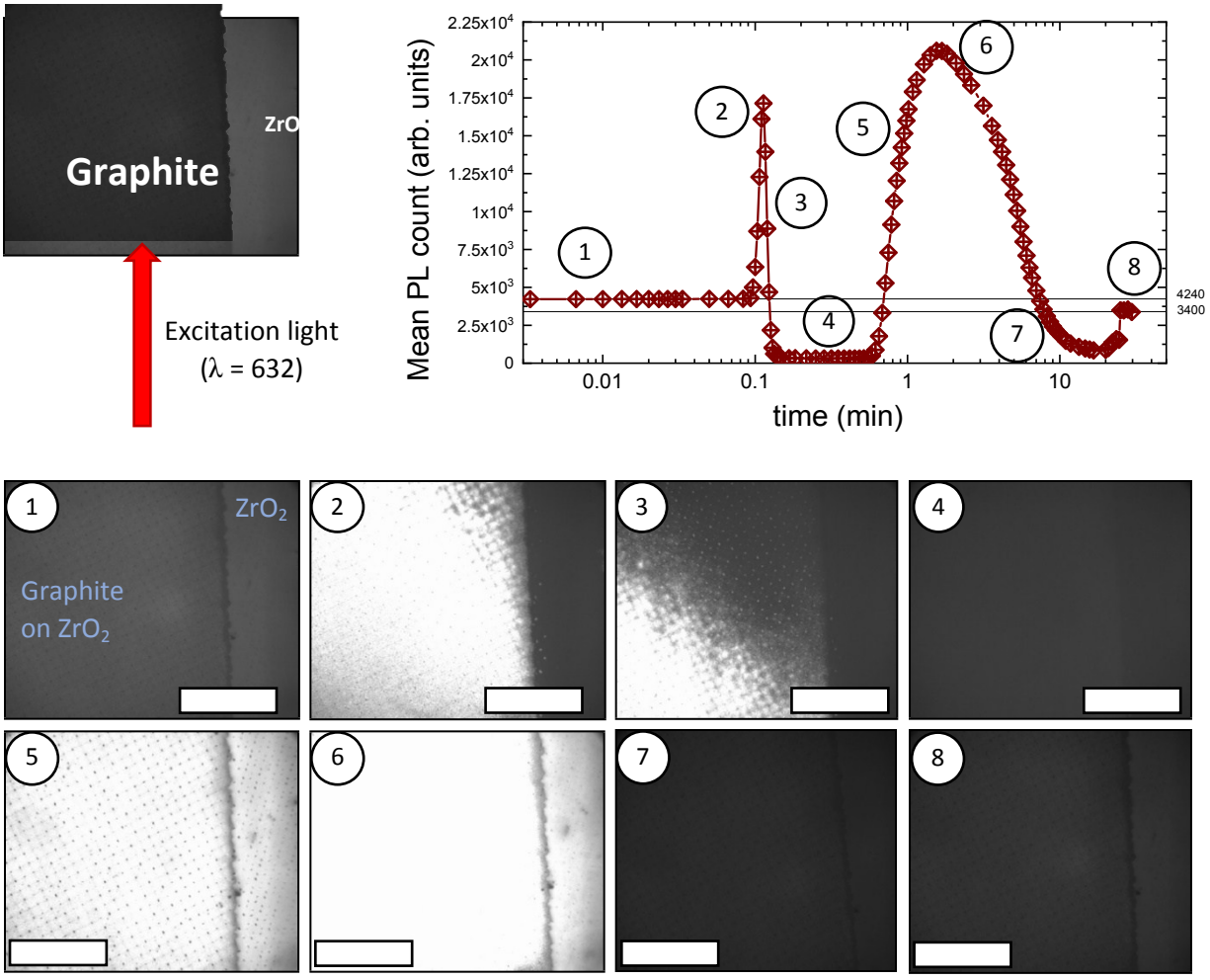

Figure S5: Real-time Photoluminescence measurement of the porous ZrO_2 and Graphite layers filled with perovskite. The PL images below correspond to different stages of the complex formation and recrystallization during the real-time measurement, according to the numbers 1-8: (1) Initial $MAPbI_3$ (2) introduction of MA^0 – passivation of vacancies and dangling bonds at the grain boundaries by MA^0 (3) Reduction of photo-active layer during $[PbMA^0{}_4I]I$ complex formation (4) Liquefied state due to excess of MA^0 – no ABX_3 structure (5) Recrystallization of $MAPbI_3$ during the removal of MA^0 from the sample. Note that the PL signal here is high, suggesting the strong passivation of residual MA0 in the sample, which indicates strong similarities during the liquefaction and crystallization processes (6) Peak of PL indicates the that the highest number of perovskite crystals has been reached and that the removal of MA^0 now only leads to increase in surface recombination (7) the excess of MA^0 is removed from the sample (8) Slightly increased PL corresponds to grain coarsening effect during the relaxation of Pb-I-Pb bonds. Scale bar – 300µm.

The PL counts in the graph above (Fig. S4) show the mean PL over the entire region of overlapped layers of ZrO_2 and Graphite. For a complete process showing the liquefaction and subsequent recrystallization please check the Video S1 in the Supplementary Materials, which shows the stages 1-6.

The evaluation of amount of methylamine gas per mole of perovskite (xMA^0) has been done using a non-ideal gas (van der Waals equation of state) equation using a correction accounting for volume occupied by gas molecules and intermolecular forces: [1]

$$\left[P + a\left(\frac{n}{V}\right)^2\right](V - nb) = nRT$$

Where P – gas pressure (which is measured using a gauge), n – moles of MA^0 gas, V – volume occupied by the gas, R – Gas constant ($8.31446 \cdot 10^{-2}$ L·bar·K^{-1}·mol^{-1}), T is temperature. a is a correction factor for the intermolecular forces and b is for adjustment due to volume occupied by the gas particles. The values for a and b were found in the reference source.[2]

The system of gas supply is presented in Fig.S7a-b. The methylamine was firstly supplied to the glass column, where the flow was controlled by valves as depicted on Figure 4.1. For filling valves 1,2 and 4 have to be open and valve 3 should be set in such position to block the gas flow to the exhaust. When the column is filled, it has to be disconnected from the system, which means that the valves 1,2,4 are closed and the valve 3 is set into position where all the pipes are connected together in order to allow the leftover Methylamine in the pipes to be removed. The gas flow during the process of filling the column with methylamine and removing the methylamine from the pipes is depicted with green and purple arrows respectively. Later the column was transported to the location where cell filling takes place. Then, the glass column was connected to vial with perovskite powder, supplying MA to the vial as it is shown in Figure 4.2. The final solution was produced by exposing perovskite to MA gas in a 1.5 mL vial in addition to Acetonitrile as an agent to reduce viscosity of solution.

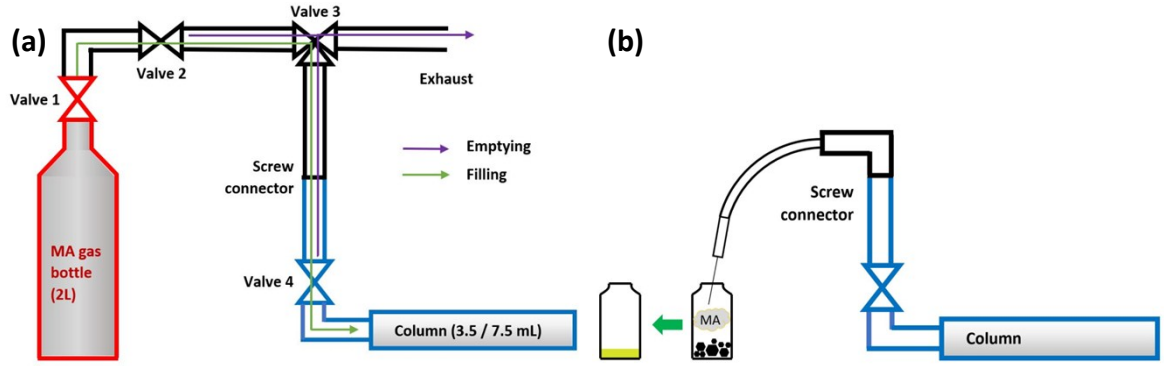

Figure S6: (a) Illustration of the station used to fill the gas column (a buffer later used for supplying MA to perovskite in (b)). The arrows indicate the gas flow of filling process and then the process of releasing MA in the pipes to the exhaust. Illustration of "melting the perovskite" process to create solution for filling the cells (b)

In such method, we were able to produce solution with various and controllable xMA^0. The values are presented in a table below:

Table S2: Evaluated amount of supplied MA^0 gas to the perovskite powder in planar and mesoporous layers

In planar films	
Perovskite mass (mg)	x – mol(MA^0)/mol(PVSK)
35.2	11.5
28.16	14.4
21.12	19.2

In the mesoporous layers	
Perovskite mass (mg)	x – mol(MA^0)/mol(PVSK)
46.9	8.6
36.4	11.1
27.4	14.8
22.26	18.2

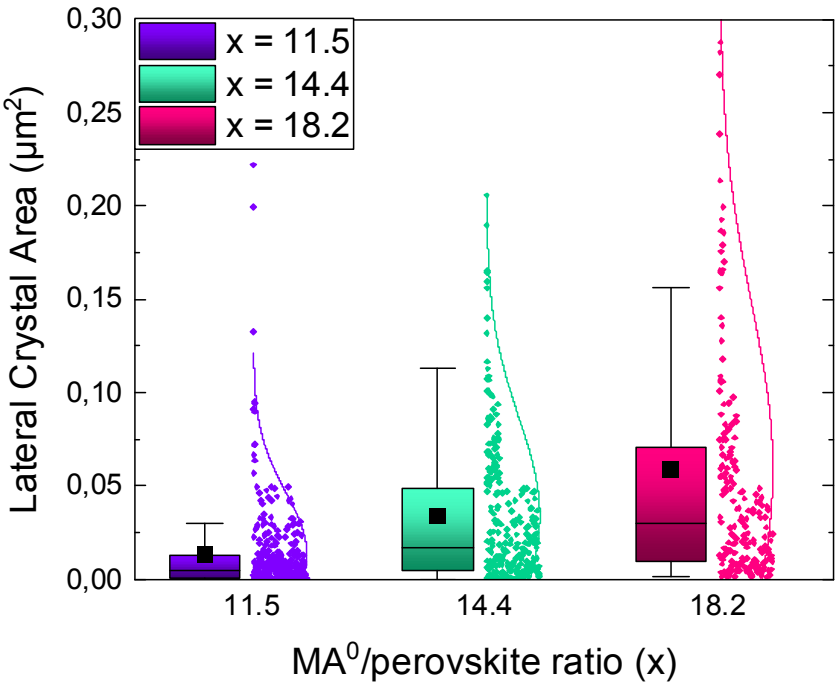

Figure S7: Crystal size distribution obtained by analyzing SEM images of the perovskite films with various MA^0/perovskite ratios using ImageJ software. The crystals were isolated by applying FFT filter, adjusting the threshold, noise correction and using embedded particle analysis plug-in. The black boxes denote the mean value of lateral crystal area, which increases with higher MA^0/perovskite ratio in the complex

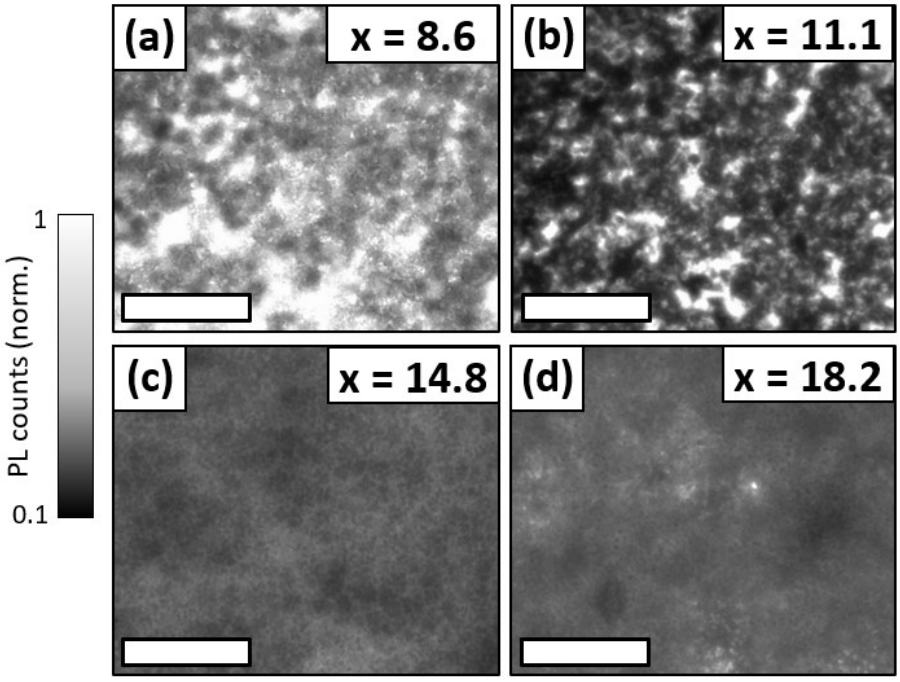

Figure S8: PL images of absorber layers crystallized from solutions with various concentrations of MA^0 inside mesoporous ZrO_2 layers (a-d). The white scale bar represents 300 µm

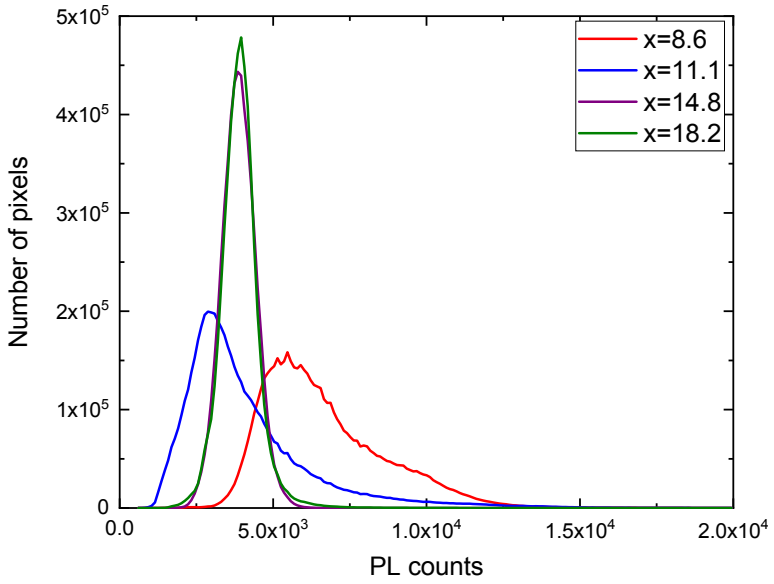

Figure S9: PL counts distribution from the PL images shown in Fig. 5

To quantify the homogeneity (*h*) of the PL image we propose to use the following relationship:

$$h = \frac{n_{max}}{\int_{\varphi_{min}}^{\varphi_{max}} n(\varphi)\, d\varphi}$$

Where the n_{max}, describing the number of pixels with the most frequently occurring local PL intensity is divided by the integrated area under the distribution curve of PL signals (here denoted as φ), which can be found in Figure S9.

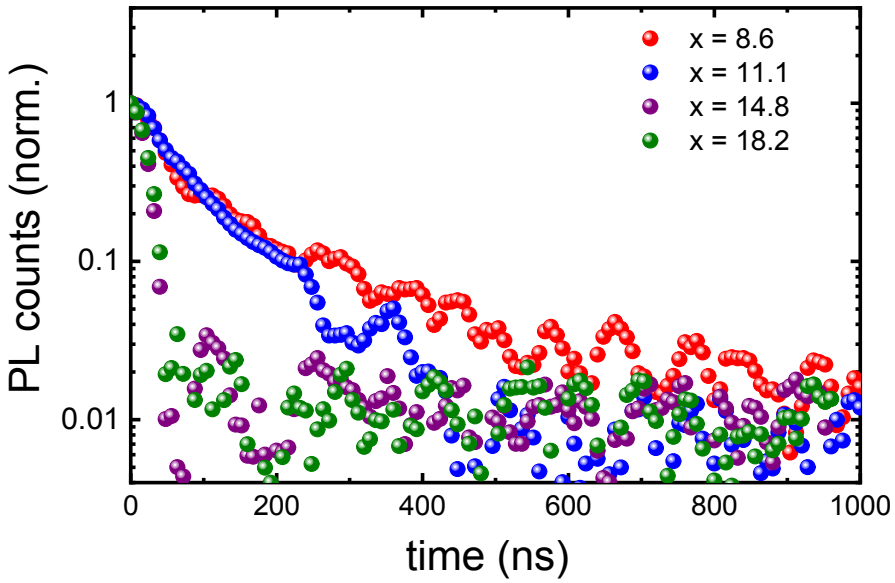

Figure S10: Time-resolved photoluminescence on the perovskite in porous ZrO_2 layers (i.e. without a quencher) produced using different x in the $MAPbI_3xMA^0$

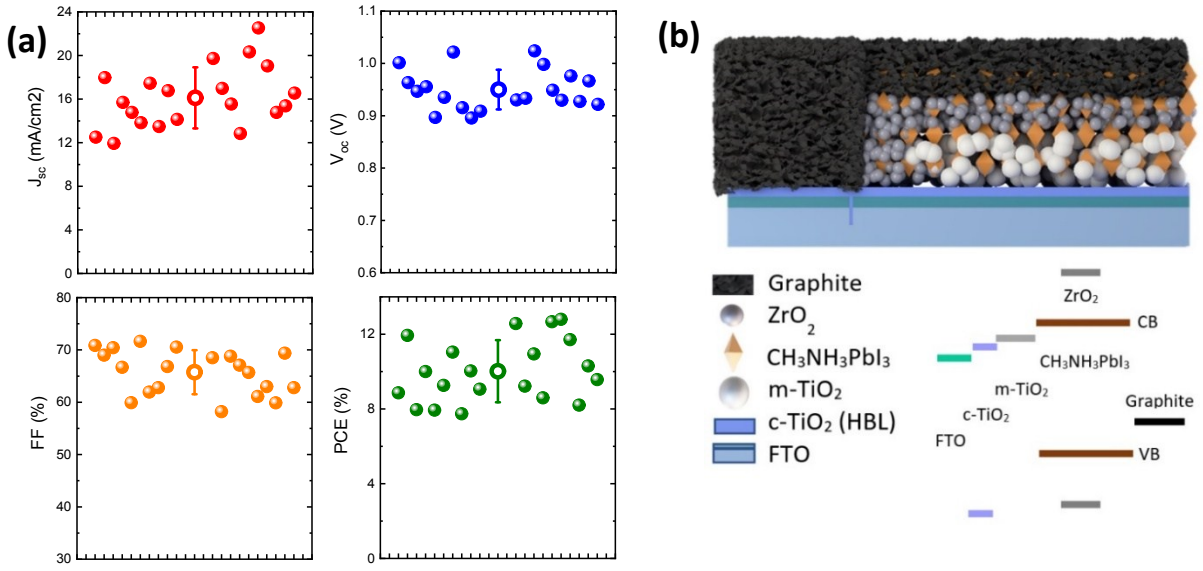

Figure S11: I-V parameters of the graphite-based perovskite solar cells produced using an optimal xMA^0, showing a high V_{oc} (a). G-PSC structure with a corresponding band diagram (b). Note that even without hole-transport material, some cells have V_{oc} above 1V, suggesting that low number of charge carriers recombine non-radiatively.

References

(1) Silbey, R. J.; Alberty, R. A.; Bawendi, M. G. *Physical chemistry*, 4th edition; Princeton, N.J., 2004.

(2) Chemistry Libretexts. van der Waals constants for real gases. https://chem.libretexts.org (accessed November 25, 2019).